QUANTUM GASES

Dissipation-induced structural instability and chiral dynamics in a quantum gas

Nishant Dogra*, Manuele Landini†, Katrin Kroeger, Lorenz Hruby, Tobias Donner‡, Tilman Esslinger

Dissipative and unitary processes define the evolution of a many-body system. Their interplay gives rise to dynamical phase transitions and can lead to instabilities. In this study, we observe a nonstationary state of chiral nature in a synthetic many-body system with independently controllable unitary and dissipative couplings. Our experiment is based on a spinor Bose gas interacting with an optical resonator. Orthogonal quadratures of the resonator field coherently couple the Bose-Einstein condensate to two different atomic spatial modes, whereas the dispersive effect of the resonator losses mediates a dissipative coupling between these modes. In a regime of dominant dissipative coupling, we observe the chiral evolution and relate it to a positional instability.

In a many-body system, unitary processes generally give rise to coherent evolution, whereas dissipative processes lead to stationary states (*1*). The interplay of these two types of processes in a driven-dissipative setting can influence a many-body system in profound ways. Examples are dissipative phase transitions (*2*–*9*), the emergence of new universality classes (*10*, *11*), dissipation-induced topological effects (*12*), complex dynamics (*13*), and the splitting of multicritical points (*14*). In this study, we observe a phenomenon in which chiral nonstationary dynamics emerges if the energy scales of dissipative and unitary processes are similar. In our experiment, we use a quantum gas to create a driven many-body system with controllable unitary and dissipative couplings. This allows us to explore the system's macroscopic behavior at the boundary between stationary and nonstationary states. We gain a conceptual understanding of the observed dynamics by considering dissipation as a structure-dependent force, analogous to mechanical nonconservative positional forces (*15*–*17*). In addition, our observations permit us to draw connections to limit cycles (*18*, *19*).

Our experiment consists of a spinor Bose-Einstein condensate (BEC) of two different Zeeman states that is coherently coupled to two different spatial atomic configurations (*20*): One coupling induces a density mode (DM) in which the density of the gas shows a checkerboard modulation, whereas the other coupling favors a spin mode (SM) in which the gas instead develops a checkerboard modulation of the spin degree of freedom (unit cells are shown in Fig. 1A). These coherent couplings are mediated via photons scattered by the atomic system from a standing-wave transverse pump laser field into a high-finesse optical cavity mode (Fig. 1B). The DM and the SM interact with orthogonal quadratures of the cavity mode. We engineer a dissipative coupling in this system, exploiting the finite cavity decay rate κ and the associated phase shift of the intracavity field across the cavity resonance: The light field scattered from the pump into the cavity acquires a phase shift ϕ_κ that effectively mixes the orthogonal quadratures, giving rise to a dissipative coupling between the DM and the SM (Fig. 1, A and B).

The strengths λ_D and λ_S of the coherent couplings between the BEC and the DM or the SM, respectively, are tuned by the lattice depth V_{TP} and polarization angle φ of the transverse pump (*20*). These couplings soften the effective excitation frequencies ω_D and ω_S of both modes, such that at a critical lattice depth the frequency of the more strongly coupled mode vanishes. This mode can then be macroscopically occupied, and the system undergoes a self-organization phase transition (*21*), breaking a spatial Z(2) symmetry. Simultaneously, the corresponding quadrature of the cavity mode is coherently populated, which we detect with a heterodyne detection system analyzing the light field leaking from the cavity (*22*).

The cavity-induced phase shift ϕ_κ and hence the dissipative coupling strength K^2 between

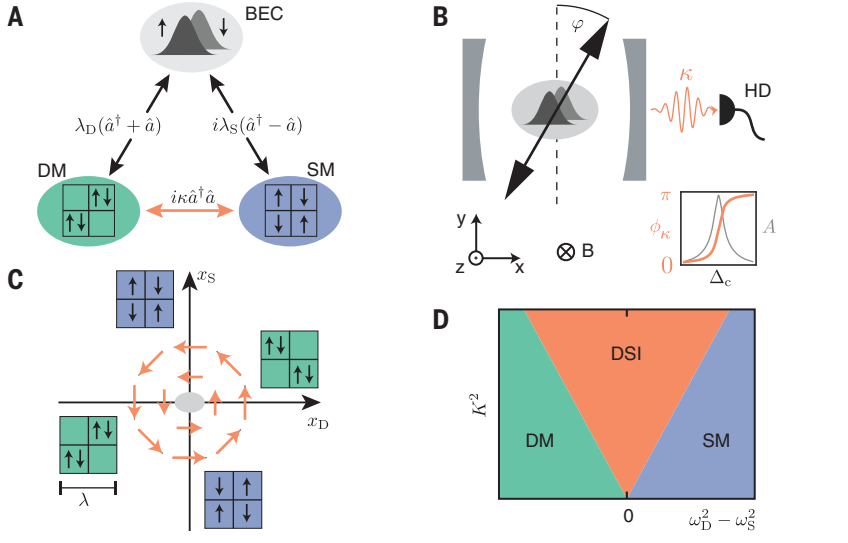

Fig. 1. Engineered dissipative coupling. (**A**) A spinor BEC containing a mixture of two Zeeman states (depicted by up and down arrows) is coherently coupled with rates λ_D and λ_S to a DM and an SM, respectively, via the two quadratures of a cavity field with annihilation operator $\hat{a}$. A dissipative coupling (orange arrow) between DM and SM is induced by the phase response of the cavity. Occupation of the DM (SM) leads to a density (spin) modulation, displayed as atoms occupying the same (opposite) checkerboard lattice sites of an exemplary green (blue) two-by-two square unit cell of dimensions λ by λ, where λ is the wavelength of the transverse pump field (see below). (**B**) The spinor BEC is coupled with a cavity mode and irradiated by a standing-wave transverse pump in the z direction with linear polarization (black arrow) at angle φ with respect to the y direction. The magnetic field B is oriented along the z direction. Light leaking out of the cavity at decay rate κ is analyzed via a heterodyne detector (HD). (Inset) Phase ϕ_κ and amplitude A response of the cavity as a function of detuning Δ_c. (**C**) Dissipation acts like a chiral force (orange); here, x_D (x_S) represents the amplitude of the density (spin) modulation. (**D**) Schematic representation of three different regimes as a function of dissipative coupling strength K^2 and detuning between the frequencies ω_D and ω_S of the DM and SM, respectively. The green (blue) region represents the DM (SM) being dominantly coupled to the spinor BEC.

Institute for Quantum Electronics, ETH Zurich, CH-8093 Zurich, Switzerland.
*Present address: Cavendish Laboratory, University of Cambridge, Cambridge CB3 0HE, UK. †Present address: Institut für Experimentalphysik und Zentrum für Quantenphysik, Universität Innsbruck, 6020 Innsbruck, Austria.
‡Corresponding author. Email: donner@phys.ethz.ch

the two modes can be controlled by the detuning Δ_c between the cavity resonance and the frequency of the transverse pump (*23*). The effect of this dissipative coupling can be understood in the x_D-x_S plane, where x_D and x_S represent the amplitudes of the density and spin modulation [see below and (*23*)] caused by the occupation of DM and SM, respectively (Fig. 1C). In this plane, the dissipative coupling acts as a force field that favors a rotation of the system's state around the origin: If the DM and the SM are degenerate, even an infinitesimally small dissipative coupling leads to a dissipation-induced structural instability (DSI) in which the system rotates with fixed chirality between the different atomic modes. The strength of the resulting force field increases with the strength of the dissipative coupling, such that the instability occurs also for increasingly nondegenerate modes, as qualitatively shown by the broadening of the DSI region in the schematic in Fig. 1D.

We prepare the ^{87}Rb spinor BEC with $N = (23 \pm 2) \times 10^3$ atoms in each of the different Zeeman states $|F = 1, m_F = \pm 1\rangle$, where F and m_F denote the total angular momentum and the corresponding magnetic quantum number, respectively. We linearly ramp up the lattice depth of the transverse pump in 50 ms and analyze the cavity output with our heterodyne setup. In Fig. 2, A and B, we show the mean photon number n_{ph} and phase ϕ (modulo 2π)

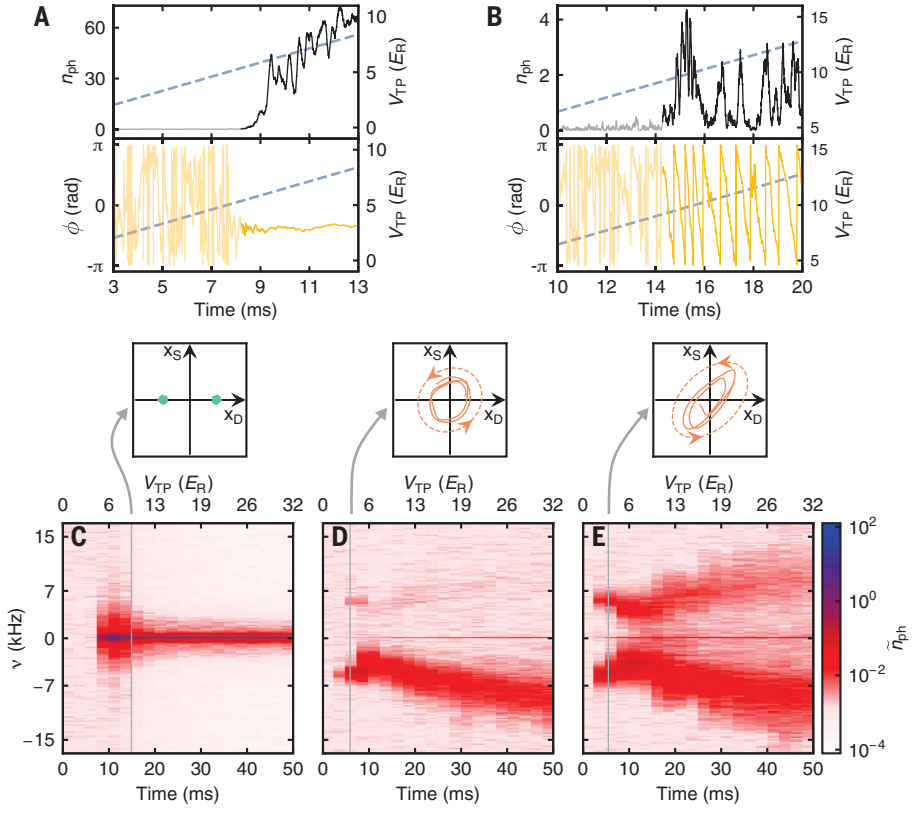

Fig. 2. Detection of the DSI. (**A** and **B**) Time evolution of the mean number of photons n_{ph} (black) in the cavity and the corresponding phase φ modulo 2π (orange) for (A) $\varphi = 58.3(1.0)°$, $\tilde{\Delta}_c/2\pi = -5.5(1)$MHz and (B) $\varphi = 63.3(1.0)°$, $\tilde{\Delta}_c/2\pi = -5.5(1)$MHz. The detuning $\tilde{\Delta}_c$ includes the effect of the atomic dispersive shift on the detuning Δ_c (*23*). The linear ramp of the lattice depth V_{TP} of the transverse pump is shown as dashed blue line. Gray and light orange lines correspond to zero occupation of the cavity. (**C** to **E**) Spectrograms showing the mean number of photons $\tilde{n}_{ph}$ as a function of frequency ν and time for (C) $\varphi = 58.3(1.0)°$, $\tilde{\Delta}_c/2\pi = -5.4(2)$ MHz; (D) $\varphi = 63.3(1.0)°$, $\tilde{\Delta}_c/2\pi = -2.5(2)$ MHz; and (E) $\varphi = 58.3(1.0)°$, $\tilde{\Delta}_c/2\pi = -2.4(2)$ MHz. A window size of 5 ms is used to construct the spectrograms, and each data set is averaged over 20 experimental realizations. Frequency ν is defined relative to the transverse pump. Corresponding insets show the evolution of the atomic state in the x_D-x_S plane extracted from the spectrograms in a duration of 500 μs at the position of the gray lines. In the inset to (C), we plot the data and its mirror about x_S to illustrate the Z(2) symmetry breaking of the self-organization phase transition. Dashed lines in the insets to (D) and (E) are the qualitative predictions of the noninteracting theory for vanishing gain (Eq. 3). All insets are rescaled with respect to each other and the theoretical lines for better visibility. Linecuts through spectrograms for similar data are presented in (*23*).

of the intracavity light field for two different sets of parameters. We find two qualitatively different behaviors: Above a critical pump power, the cavity field has a nonzero amplitude and either a well-defined (Fig. 2A) or a monotonically changing phase (modulo 2π; Fig. 2B). A well-defined phase indicates that only one quadrature of the cavity field is excited, corresponding to either the SM or the DM being populated, which is determined by the prevailing coherent coupling. In contrast, a monotonically changing phase is observed when the dissipative coupling is dominant and signals that the system is continuously evolving through the different spatial modes linked with the two quadratures of the cavity field.

The many-body Hamiltonian of the system is given by

$$\hat{H} = -\hbar\Delta_c\hat{a}^\dagger\hat{a} + \hbar\omega_0(\hat{J}_{z,+} + \hat{J}_{z,-}) + \frac{\hbar}{\sqrt{N}}\left[\lambda_D(\hat{a}^\dagger + \hat{a})(\hat{J}_{x,+} + \hat{J}_{x,-}) - i\lambda_S(\hat{a}^\dagger - \hat{a})(\hat{J}_{x,+} - \hat{J}_{x,-})\right] \quad (1)$$

where $\hat{a}(\hat{a}^\dagger)$ is the annihilation (creation) operator corresponding to the y-polarized cavity mode in the frame of the transverse pump frequency. The atomic system is represented by an ensemble of N effective "spins" in each of the two Zeeman states (labeled with ±), with $\hat{J}_{x,\pm}$, $\hat{J}_{y,\pm}$, and $\hat{J}_{z\pm}$ being the corresponding angular momentum operators. This pseudo-spin is constructed from the macroscopically occupied zero momentum state $|0\rangle$ of the BEC and an excited state $|k\rangle$ with a symmetric superposition of four momentum states $|p_x = \pm\hbar k,\ p_z = \pm\hbar k\rangle$, which represent one recoil momentum $\hbar k$ each in the cavity and the transverse pump direction (*21*). The wave number of the transverse laser field with wavelength λ is given by $k = 2\pi/\lambda$. For zero lattice depth V_{TP} of the transverse pump, the energy difference between the states $|0\rangle$ and $|k\rangle$ is $\hbar\omega_0 = 2E_R = \hbar^2k^2/m$, where m is the mass of a ^{87}Rb atom and $\hbar$ is Planck's constant divided by 2π. The first two terms in Eq. 1 describe the energies of the bare photonic and atomic modes, respectively, whereas the third term captures the couplings of the DM and the SM to the respective quadratures of the cavity field (*23*). In this framework, the amplitudes of the DM and the SM are given by $x_D = \frac{1}{N}(\langle\hat{J}_{x,+}\rangle + \langle\hat{J}_{x,-}\rangle)$ and $x_S = \frac{1}{N}(\langle\hat{J}_{x,+}\rangle - \langle\hat{J}_{x,-}\rangle)$, respectively.

The damping of the cavity mode can be modeled by a decay term $-\kappa\hat{a}^\dagger$ in the equation of motion of the operator $\hat{a}^\dagger$. It causes a phase shift $\phi_\kappa = \tan^{-1}(-\kappa/\Delta_c)$ of the field scattered into the cavity by the atomic system. We adiabatically eliminate the cavity field and write the linearized equations of motion near the ground state of the noninteracting

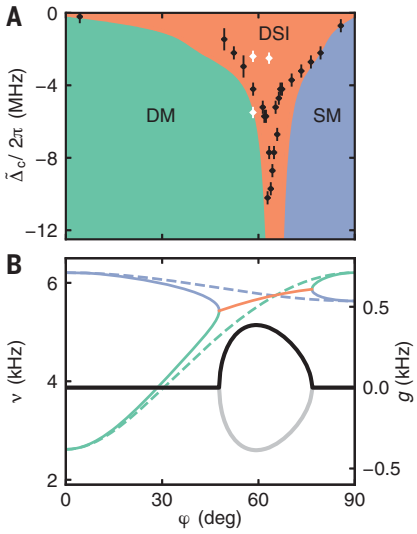

Fig. 3. Boundary of the instability-dominated regime. (**A**) Critical detuning, including the dispersive shift (*23*), for the onset of the dissipation-induced instability as a function of polarization angle φ. The black data points indicate the smallest detuning, where the strength of the sidebands becomes larger than the signal at the transverse pump frequency in the spectrograms for a fixed lattice depth of $21E_R$. The white diamonds indicate the parameters for the spectrograms shown in Fig. 2, C to E. Error bars are given by the discretized detuning interval in which the transition was detected. The polarization angle determination has an error of 1°. The green and blue regions correspond to DM and SM being respectively more strongly coupled to the spinor BEC. In the orange region, the system is dominated by the dissipation-induced instability. The boundary between different regions is obtained from a noninteracting theory [see main text and (*23*)]. (**B**) Green and blue solid (dashed) lines show the frequency ν of the two eigenmodes of the system as a function of the polarization angle in the presence (absence) of dissipative coupling. Without dissipation, the two modes are the DM (green) and the SM (blue). Dissipation leads to level attraction between the two modes and hence changes their frequencies. In the instability-dominated regime, the two modes are synchronized (orange). Correspondingly, the gains g of the amplified mode (black) and the damped mode (gray) are plotted. The lines are drawn for $\tilde{\Delta}_c/2\pi = -2.7$MHz or $\Delta_c/2\pi = -4$MHz and $V_{TP} = 1.5E_R$.

spinor BEC for the average amplitudes x_D and x_S (*23*)

$$\frac{d^2}{dt^2}\begin{pmatrix} x_D \\ x_S \end{pmatrix} = \begin{pmatrix} -\omega_D^2 & -K^2 \\ K^2 & -\omega_S^2 \end{pmatrix}\begin{pmatrix} x_D \\ x_S \end{pmatrix} \quad (2)$$

where $\omega_D^2 - \omega_S^2 \propto \sin\delta\phi$ with $\delta\phi = 2\tan^{-1}(\lambda_S/\lambda_D) - \pi/2$ is a measure of the relative coupling strength of the BEC to the SM and the DM. The strength of the dissipative coupling $K^2 \propto V_{TP}\sin^2\phi_\kappa\cos\delta\phi$ can thus be enhanced by either increasing the cavity-induced phase shift or making the two modes degenerate. This dissipative coupling generates a chiral force orthogonal to the current position vector of the system in the x_D-x_S plane (Fig. 1C) and provides an example of a positional force (*17*, *24*). Such positional forces are known in mechanical systems such as a rotating shaft subject to friction caused by an incompressible viscous fluid in a bearing. The incompressibility of the fluid leads to unequal frictional forces on opposite sides of the shaft, resulting in a positional force orthogonal to the direction of the displacement (*15*, *16*). These positional forces represent the only possible linear mechanical forces besides conservative trapping forces, centripetal forces, and frictional forces (*23*). In our system, when the two atomic modes are degenerate, this positional force cannot be counteracted by the restoring harmonic force pointing toward the origin, thus leading to a dissipation-induced structural or positional instability (*17*, *24*, *25*).

Mode degeneracy (i.e., $\lambda_D = \lambda_S$ such that $\delta\phi = 0$) is reached at the critical polarization angle $\varphi_c = 65.1°$ for the chosen wavelength of the transverse pump of λ = 784.7 nm. To explain our observations, we analyze the solutions of Eq. 2 and the corresponding intracavity light field for polarization angles close to φ_c—that is, for a small $\delta\phi$ (*23*)

$$[x_D^c, x_S^c] = A\left[\cos\omega t, \sin\left(\omega t + \frac{\Delta_c}{\kappa}\delta\phi\right)\right]e^{gt}$$

$$\langle \hat{a}^\dagger \rangle \propto (x_D^c - ix_S^c) - \frac{\delta\phi}{2}(x_D^c + ix_S^c)$$
$$\propto A\left[e^{-i\omega t} - \frac{\delta\phi}{2}\left(1 + i\frac{\Delta_c}{\kappa}\right)e^{i\omega t}\right]e^{gt} \quad (3)$$

In the limit $\delta\phi = 0$, this time-dependent solution implies that the system is rotating in the x_D-x_S plane with fixed chirality at frequency ω and amplification rate g (additionally, t is time and A is the amplitude at t=0) (*23*). Microscopically, this rotation is associated with the atomic spins moving from one λ-periodic spatial pattern to another (Fig. 1C). Because the two atomic modes are connected to different quadratures of the cavity, the phase of the cavity field evolves monotonically, as observed in Fig. 2B and shown in Eq. 3.

The frequency spectrum of the light leaking from the cavity is also accessible with our heterodyne setup (*22*). Figure 2, C to E, shows spectrograms for three different sets of parameters of data similar to Fig. 2, A and B, but averaged over 20 repetitions. Figure 2C shows a spectrogram where the signal is located at zero frequency (ν = 0). It corresponds to the frequency of the transverse pump and is identical to the observation of a constant time phase of the cavity field, as shown in Fig. 2A. We identify this as the formation of a static checkerboard density pattern that coherently scatters the pump field into the cavity (*20*, *23*). The corresponding steady state of the system is displayed in the inset to Fig. 2C.

In contrast, Figs. 2, D and E, depict red (ν < 0) and blue (ν > 0) detuned sidebands with the peak frequency being a function of the lattice depth of the transverse pump. Observation of only a red sideband, as in Fig. 2D, is equivalent to a linearly running phase. For small lattice depths ($V_{TP} < 6E_R$), the sideband frequency is expected to be close to the root mean square ω_e of the two mode frequencies—that is, $\omega \approx \omega_e = \sqrt{(\omega_D^2 + \omega_S^2)/2}$. Evolution at this intermediate frequency reflects a synchronization process (*26*) between the two spatial modes arising from the dissipative coupling. For large lattice depths, the sideband frequency depends on the dissipative coupling strength: $\omega \approx K^2/2|\omega_e|$ (*23*). In this limit, the two mode frequencies become imaginary, corresponding to the self-organization phase transition in the absence of dissipative coupling.

The relative strength R of the blue with respect to the red sideband increases toward 1 as φ deviates from the critical angle φ_c. The presence of the blue sideband is connected to nonzero $\delta\phi$ (Eq. 3) and leads to an elliptical evolution in the x_D-x_S plane. The relative strength R, and hence the ellipticity of the chiral solution, can be influenced via Δ_c or $|\delta\phi|$. Microscopically, the blue sideband is connected to the motion of a different number of atoms in each Zeeman state. The insets to Fig. 2, D and E, show data of the time-varying trajectory of the system together with solutions obtained from Eq. 2 for $g = 0$, illustrating the nonstationary chiral state. When preparing the system in the DSI at a fixed lattice depth, we observe a narrow red sideband that persists over tens of milliseconds (*23*), corresponding to a uniform circular motion in the x_D-x_S plane. This observation hints at the presence of a limit cycle in our system (*18*, *19*).

Our mean-field description of the system in terms of a positional instability does not describe all aspects of the observed dynamics. For example, the number of photons in the case of the DSI (Fig. 2, D and E) is much smaller than during self-organization (Fig. 2C), although the instability is associated with a finite amplification rate g. Even the limit cycle–like behavior persisted for a long time without much increase in the corresponding amplitude. Moreover, there is a finite lattice depth threshold for the onset of the DSI (Fig. 2B), although g is positive for infinitesimal lattice depths. We attribute this, as well as the observed pulsing behavior in the number of photons (Fig. 2B), to collisional interactions between the atoms (*23*). Such a behavior of collisional interactions can possibly be modeled as an atomic

dissipation channel that competes with the cavity-induced instability. Similar competitions between multiple heat baths are predicted to give rise to dissipative frustration (*27*, *28*).

We experimentally map out the boundary of the DSI region by ramping up the transverse pump lattice to $25E_R$ in 50 ms for various polarization angles φ and detunings Δ_c (Fig. 3A). For a given polarization angle, we define the onset of the DSI by the minimum detuning where the strength of the sidebands exceeds the signal at the transverse pump frequency. We theoretically obtain the boundary of the DSI (orange region in Fig. 3A) from Eq. 2 as $|\omega_D^2 - \omega_S^2| = 2K^2$, which results in a critical detuning $\Delta_{c,b} = -\kappa/\tan|\delta\phi|$. A study of the extent of the DSI as a function of polarization angle and transverse pump lattice depth is presented in (*23*).

Physically, the boundary of the DSI can be understood as the onset of synchronization between DM and SM. Such a synchronization process is the result of a dissipation-induced level attraction, a hallmark of non-Hermitian systems (*29*, *30*). Figure 3B shows the frequencies of the DM and SM in the absence (dashed lines) and presence (solid lines) of dissipation. In the vicinity of the critical angle, this level attraction leads to the emergence of two degenerate modes with opposite chirality. Whereas one of these modes is damped, the other is amplified, which gives rise to the DSI. Similar forms of level attraction leading to instability are observed in optomechanical systems (*31*) and, in general, in non-Hermitian photonic systems, where they can be associated with parity–time symmetry-breaking phase transitions (*30*) and exceptional points (*32*, *33*). We have experimentally studied a many-body system in which both coherent and dissipative couplings are independently tunable. Our observation of a dissipation-induced instability represents a form of quantum many-body dynamics that shares characteristics with but is distinct from limit cycles (*18*, *19*, *34*) and time crystals (*35*, *36*).

REFERENCES AND NOTES

1. H.-P. Breuer, F. Petruccione, *The Theory of Open Quantum Systems* (Oxford Univ. Press, 2002).
2. N. Syassen *et al*., *Science* **320**, 1329–1331 (2008).
3. G. Barontini *et al*., *Phys. Rev. Lett.* **110**, 035302 (2013).
4. F. Brennecke *et al*., *Proc. Natl. Acad. Sci. U.S.A.* **110**, 11763–11767 (2013).
5. R. Labouvie, B. Santra, S. Heun, H. Ott, *Phys. Rev. Lett.* **116**, 235302 (2016).
6. T. Tomita, S. Nakajima, I. Danshita, Y. Takasu, Y. Takahashi, *Sci. Adv.* **3**, e1701513 (2017).
7. I. Carusotto, C. Ciuti, *Rev. Mod. Phys.* **85**, 299–366 (2013).
8. T. Fink, A. Schade, S. Höfling, C. Schneider, A. Imamoglu, *Nat. Phys.* **14**, 365–369 (2018).
9. J. T. Young, A. V. Gorshkov, M. Foss-Feig, M. F. Maghrebi, arXiv:1903.02569 [cond-mat.quant-gas] (6 March 2019).
10. S. Diehl, A. Tomadin, A. Micheli, R. Fazio, P. Zoller, *Phys. Rev. Lett.* **105**, 015702 (2010).
11. D. Nagy, G. Szirmai, P. Domokos, *Phys. Rev. A* **84**, 043637 (2011).
12. S. Diehl, E. Rico, M. A. Baranov, P. Zoller, *Nat. Phys.* **7**, 971–977 (2011).
13. B. Buča, J. Tindall, D. Jaksch, *Nat. Commun.* **10**, 1730 (2019).
14. M. Soriente, T. Donner, R. Chitra, O. Zilberberg, *Phys. Rev. Lett.* **120**, 183603 (2018).
15. B. L. Newkirk, H. Taylor, *Gen. Electr. Rev.* **28**, 559–568 (1925).
16. P. L. Kapitsa, *Zh. Tekh. Fiz.* **9**, 124–147 (1939).
17. D. R. Merkin, *Introduction to the Theory of Stability* (Springer, 1996).
18. F. Piazza, H. Ritsch, *Phys. Rev. Lett.* **115**, 163601 (2015).
19. E. I. Rodríguez Chiacchio, A. Nunnenkamp, *Phys. Rev. Lett.* **122**, 193605 (2019).
20. M. Landini *et al*., *Phys. Rev. Lett.* **120**, 223602 (2018).
21. K. Baumann, C. Guerlin, F. Brennecke, T. Esslinger, *Nature* **464**, 1301–1306 (2010).
22. R. Landig, F. Brennecke, R. Mottl, T. Donner, T. Esslinger, *Nat. Commun.* **6**, 7046 (2015).
23. Supplementary materials.
24. R. Krechetnikov, J. E. Marsden, *Rev. Mod. Phys.* **79**, 519–553 (2007).
25. S. H. Crandall, in "Rotordynamic Instability Problems in High-Performance Turbomachinery" (NASA Conference Publications 2133, NASA, 1982), vol. 2250, pp. 274–283.
26. A. Pikovsky, M. Rosenblum, J. Kurths, *Synchronization: A Universal Concept in Nonlinear Science* (Cambridge Univ. Press, 2003).
27. H. Kohler, F. Sols, *New J. Phys.* **8**, 149 (2006).
28. D. Maile, S. Andergassen, W. Belzig, G. Rastelli, *Phys. Rev. B* **97**, 155427 (2018).
29. I. Rotter, *J. Phys. A Math. Theor.* **42**, 153001 (2009).
30. R. El-Ganainy *et al*., *Nat. Phys.* **14**, 11–19 (2018).
31. N. R. Bernier, L. D. Tóth, A. K. Feofanov, T. J. Kippenberg, *Phys. Rev. A* **98**, 023841 (2018).
32. W. D. Heiss, *J. Phys. A Math. Theor.* **45**, 444016 (2012).
33. M.-A. Miri, A. Alù, *Science* **363**, eaar7709 (2019).
34. M. Gutzwiller, *Chaos in Classical and Quantum Mechanics* (Springer, 1990).
35. J. Zhang *et al*., *Nature* **543**, 217–220 (2017).
36. S. Choi *et al*., *Nature* **543**, 221–225 (2017).
37. N. Dogra, M. Landini, K. Kroeger, L. Hruby, T. Donner, T. Esslinger, "Dissipation Induced Structural Instability and Chiral Dynamics in a Quantum Gas," ETH Zurich Research Collection (2019); https://doi.org/10.3929/ethz-b-000366051.

ACKNOWLEDGMENTS

We thank B. Buca, E. Rodriguez Chiacchio, F. Ferri, D. Jaksch, A. Nunnenkamp, and J. Tindall for discussions. **Funding:** We acknowledge funding from SNF [project nos. 182650 and 175329 (NAQUAS QuantERA) and NCCR QSIT], EU Horizon 2020 [ERC Advanced Grant TransQ (project no. 742579)], and SBFI (QUIC, contract no. 15.0019). **Author contributions:** N.D., M.L., K.K., and L.H. prepared the experiment and collected the data; N.D., M.L., and K.K. evaluated the data; N.D. and M.L. developed the theory; T.D. and T.E. supervised the project; and all authors contributed to discussions and writing of the manuscript. **Competing interests:** The authors declare no competing interests. **Data and materials availability:** Data and scripts are available in the ETH Zurich Research Collection repository (*37*).

SUPPLEMENTARY MATERIALS

science.sciencemag.org/content/366/6472/1496/suppl/DC1
Materials and Methods
Supplementary Text
Figs. S1 to S5
References (*38*–*41*)

20 December 2018; accepted 6 November 2019
10.1126/science.aaw4465

Dissipation-induced structural instability and chiral dynamics in a quantum gas

Nishant Dogra, Manuele Landini, Katrin Kroeger, Lorenz Hruby, Tobias Donner and Tilman Esslinger

Science **366** (6472), 1496-1499.
DOI: 10.1126/science.aaw4465

Chirality by dissipation

Quantum many-body systems can display exotic dynamics in the presence of dissipation. Dogra *et al.* studied such dynamics in a system consisting of an atomic Bose-Einstein condensate located in an optical cavity and exposed to a standing wave of laser light. Light scattering off the atomic cloud and into the cavity resulted in two distinct, spatially patterned collective modes for the atoms. When the researchers then introduced dissipation to couple the two modes, the system followed a directed circular path through phase space, rotating between the modes.

Science, this issue p. 1496